star-Porphyrazines: Synthetic, Structural, and Spectral Investigation of Complexes of the Polynucleating Porphyrazineoctathiolato Ligand

Christopher S. Velázquez,[†] Glenn A. Fox,[†] William E. Broderick,[†] Kevin A. Andersen,[‡] Oren P. Anderson,[‡] Anthony G. M. Barrett,*[,‡] and Brian M. Hoffman*[,†]

Contribution from the Departments of Chemistry, Northwestern University, Evanston, Illinois 60208, and Colorado State University, Fort Collins, Colorado 80523.
Received September 18, 1991

Abstract: We have devised a new polynucleating porphyrinic ligand, porphyrazine-2,3,7,8,12,13,17,18-octathiolato, $(pz)(S^-)_8$, the molecular structure of which may be thought of as a porphyrazine (tetraazaporphyrin) with four dithiolene moieties peripherally fused at the β-positions. Novel *star*-porphyrazine complexes $(R_2Sn)_4$-*star*-$M(pz)(S^-)_8$ (**7a**: R = *t*-Bu, M = Ni; **7b**: R = *n*-Bu, M = Ni; **8**: R = *t*-Bu, M = Cu) have been synthesized. Complex **7a** crystallizes in the monoclinic space group $C2/c$ with 4 macrocycles and 4 ordered solvent molecules (toluene) in a unit cell of dimensions a = 21.911 (3) Å, b = 21.265 (2) Å, c = 14.882 (3) Å, and β = 94.44 (2)°. The polynucleating $(pz)(S^-)_8$ ligand in **7a** coordinates one nickel atom in the central cavity and four tin atoms around the periphery using two thiolate sulfur atoms and one meso nitrogen atom for each tin, thus providing the first example of meso nitrogen coordination observed for a porphyrazine. The crystal structure of model complex **3b**·H_2O, (aquo)(octakis(methylthio)porphyrazinato)magnesium(II), was also solved: it crystallizes in the orthorhombic space group *Pnma* with 4 molecules in a unit cell of dimensions a = 14.279 (3) Å, b = 26.403 (6) Å, and c = 8.257 (2) Å. Comparison with the least-squares plane to the porphyrazine core of **3b**·H_2O and **7a** shows that each is nearly planar and that the two have similar bond distances and angles; however, the bond angles involving the sulfur atoms of **7a** are changed significantly as a result of coordination to tin. The electronic absorption spectra of **7a**, **7b**, and **8** show a suppression of the absorbance in the Soret region due to interaction of the Sn with the meso-nitrogen lone-pair and π-orbitals. Addition of halide ions restores the Soret absorption. Halide and pseudohalide ions bind to the Sn atoms of **7b** in a two-stage manner, with first one X^- and then two X^- per Sn coordinating. Halide coordination to Sn is reversed upon dilution for X^- = Br^-, I^-, and SCN^-, but not for F^-. The evidence suggests that the Sn atoms undergo a cooperative linkage isomerization induced by halide coordination of the second halide per Sn. The EPR spectrum of 1% **8** diluted into diamagnetic host **7a** was recorded, and its features are consistent with other square-planar copper porphyrins and phthalocyanines.

Introduction

The recent interest in porphyrinic molecules substituted with pendant transition metal-containing centers stems from their redox activity,[1] electron transfer behavior,[2] magnetic interactions,[3] and valence delocalization.[4] Several different approaches to designing polynucleating porphyrins have emerged. These include meso substitution with ferrocenes[1,4] or crown ethers,[3b] as well as substitution with metal-ion-coordinating pendant-arms[3c] and basket-handles.[2b] There are also examples of *meso*-tetrapyridylporphyrins that coordinate metal ions peripherally via the pyridyl groups.[2a] However, for most of these complexes, the extent of electronic interaction between metal sites is quite low.

We have devised a new polynucleating porphyrinic ligand, porphyrazine-2,3,7,8,12,13,17,18-octathiolato, $(pz)(S^-)_8$, the molecular structure of which may be thought of as a porphyrazine (tetraazaporphyrin) with four dithiolene moieties peripherally fused at the β-positions (Figure 1). This structure should allow for the chelation of a wide range of metal ions at the periphery as well as at the center. Moreover, metal–dithiolene complexes exhibit highly delocalized pπ-based molecular orbitals, as do metalloporphyrins, and a high degree of conjugation should be experienced throughout the entire ligand. As a result of orbital interaction between the peripheral metal ions and the porphyrazine (pz) π-system,[5] the porphyrazine π-system is expected to mediate indirect metal–metal interactions.

The porphyrazineoctathiolate ligand was first suggested to exist in a series of polymerized $M(mnt)_2^{2-}$ complexes.[6] However, we have succeeded in preparing and structurally characterizing *molecular star*-porphyrazine complexes in which the porphyrazineoctathiolate ligand coordinates five metal atoms, one in the central hole and four at the periphery, and further have discovered[7] that the peripheral metals can have two distinct coordination modes: tridentate (S–N–S) and bidentate (S–S) (Figure 1). The tridentate mode presents the first example of meso nitrogen coordination observed in a porphyrazine. In this article we report the synthesis and properties of several $[R_2SN]_4$-*star*-$M(pz)S_8$ as novel compounds in their own right and as potential precursors to other peripherally metalated molecules. Details are presented of the first two crystal structures of porphyrazine complexes, $[(t\text{-Bu})_2Sn]_4$-*star*-$Ni(pz)S_8$ (**7a**) and the reference compound $Mg(omtp)(H_2O)$ (**3b**). We further discuss the dramatic effect that meso nitrogen coordination has on the electronic spectra of the porphyrazine core.

Experimental Section

Materials and Methods. THF was distilled from sodium benzophenone ketyl. Chloroform (Burdick & Jackson, amylene-stabilized) was free of ethanol. Water was passed through an ion-exchange column and distilled in a glass Corning Mega-Pure system. All other solvents were reagent grade and were used as supplied. Anhydrous ammonia (Matheson) was ultra-high-purity grade. Silica gel used for chromatography

[†] Northwestern University.
[‡] Colorado State University.

(1) Schmidt, E. S.; Calderwood, T. S.; Bruice, T. C. *Inorg. Chem.* **1986**, *25*, 3718.
(2) (a) Franco, C.; McLendon, G. *Inorg. Chem.* **1984**, *23*, 2370. (b) Hamilton, A. D.; Rubin, H. D.; Bocarsly, A. B. *J. Am. Chem. Soc.* **1984**, *106*, 7255–7257.
(3) (a) Gupta, G. P.; Lang, G.; Koch, C. A.; Wang, B.; Scheidt, W. R.; Reed, C. A. *Inorg. Chem.* **1990**, *29*, 4234–4239. (b) Hamilton, A.; Lehn, J.-M.; Sessler, J. L. *J. Am. Chem. Soc.* **1986**, *108*, 5158–5167. (c) Gunter, M. J.; Mander, L. N.; McLaughlin, G. M.; Murray, K. S.; Berry, K. J.; Clark, P. E.; Buckingham, D. A. *J. Am. Chem. Soc.* **1980**, *102*, 1470–1473.
(4) Wollman, R. G.; Hendrickson, D. N. *Inorg. Chem.* **1977**, *16*, 3079.
(5) Abbreviations: pz = porphyrazine; mnt = maleonitriledithiolate; obtp = octakis(benzylthio)porphyrazine; omtp = octakis(methylthio)porphyrazine; $(pz)(S^-)_8$ = porphyrazineoctathiolato; pc = phthalocyanine; tpp = *meso*-tetraphenylporphyrin.
(6) Manecke, G.; Wöhrle, D. *Makromol. Chem.* **1968**, *120*, 176–191.
(7) (a) Velázquez, C. S.; Broderick, W. E.; Sabat, M.; Barrett, A. G. M.; Hoffman, B. M. *J. Am. Chem. Soc.* **1990**, *112*, 7408–7410. (b) Velázquez, C. S.; Barrett, A. G. M.; Hoffman, B. M. *Abstract of Papers*, American Chemical Society, 200th National Meeting; American Chemical Society: Washington, DC, 1990; INOR 205.

0002-7863/92/1514-7416$03.00/0 © 1992 American Chemical Society

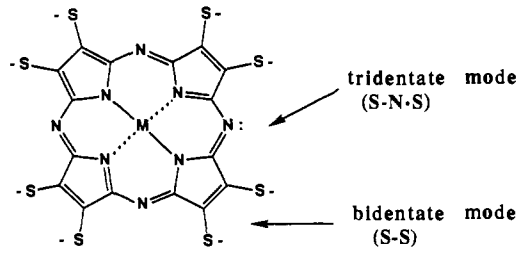

Figure 1. Coordination modes of the porphyrazineoctathiolate ligand.

Table I. Crystallographic Data for **7a**·(C_7H_8)·1.25(CH_2Cl_2)

molecular formula	$C_{48}H_{72}N_8NiS_8Sn_4 \cdot C_7H_8 \cdot 1.25(CH_2Cl_2)$
formula weight, amu	1749.40
crystal system	monoclinic
space group	$C2/c$ (No. 15)
a, Å	21.911 (3)
b, Å	21.265 (2)
c, Å	14.822 (3)
β, deg	94.44 (2)
V, Å^3	6885 (1)
Z	4
temp, °C	−120
F(000)	3456
ρ(obsd), g/cm^3	1.71 (2)
ρ(calcd), g/cm^3	1.69
crystal dimens, mm	0.25 × 0.30 × 0.40
radiation	Mo Kα (λ = 0.7101 Å)
μ, cm^{-1}	20.6
scan type	$\theta/2\theta$
2θ range, deg	$4 \le 2\theta \le 50$
total no. of reflcns	6219
no. of unique obsd reflcns	4794 ($F_o \ge 6\sigma(F_o)$)
no. of least-squares parameters	339
R	0.0288
R_w	0.0420

was Merck Kieselgel 60 (270–400 mesh). Sodium metal was freshly cut under THF immediately prior to use. Disodium maleonitriledithiolate (Na_2mnt) was prepared by the method of Davison and Holm.[8] Complex **3b** was prepared as described,[9] and single crystals were grown by slow evaporation from acetone. All other reagents were used as supplied without further purification. Schlenk-line manipulations were performed on a custom-built apparatus (W. A. Sales) with all PTFE valves (J. Young), and the nitrogen was passed through a MnO gas scrubber and a column of activated molecular sieves.[10]

^{1}H and ^{119}Sn NMR spectra were obtained using a Varian XLA-400 instrument. Electronic spectra were recorded using a Hewlett-Packard HP8452A spectrophotometer. Fast-atom bombardment mass spectra (FAB-MS) were obtained by Dr. Doris Hung using a VG-70-250E instrument. Elemental analyses were performed by Schwarzkopf Microanalytical Laboratories, Woodside, NY. Melting points were obtained using a Reichert hot-stage microscope and are uncorrected.

Electron paramagnetic resonance (EPR) spectra were measured using a modified Varian E-4 X-band spectrometer and the field was calibrated using diphenylpicrylhydrazyl (dpph) as a standard. Powder EPR samples of Cu(obtp) (**5b**) and Cu-*star*-porphyrazine (**8**) were prepared by recrystallizing about 1% of each with their corresponding diamagnetic nickel hosts from chlorobenzene and 4:1 toluene–dichloromethane, respectively.

The single-crystal X-ray diffraction data for **7a** were collected at Northwestern University using an Enraf-Nonius CAD4 diffractometer. Lorentz, polarization, and absorption corrections were applied. The structure of **7a** was solved by direct methods using the TEXSAN software package (Version 4) on a Digital Microvax 3600 workstation. All nonhydrogen atoms and all hydrogen atoms except those bonded to C14, C15, and C16 were located from the difference map; the other hydrogen atoms were included in idealized positions (C–H = 0.96 Å). The nonhydrogen atoms of the porphyrazine and the ordered toluene molecules (vide infra) were refined with anisotropic thermal parameters, and all other atoms were refined isotropically. The ordered toluenes rest on a 2-fold rotation axis, and as such, the methyl hydrogen atoms were not included in the refinement. The poorly ordered dichloromethane molecules were located near eight general positions but could not be refined

(8) Davison, A.; Holm, R. H. *Inorg. Synth.* **1967**, *6*, 8–25.
(9) Schramm, C. J.; Hoffman, B. M. *Inorg. Chem.* **1980**, *19*, 383–385.
(10) Brown, T. L. *Rev. Sci. Instr.* **1962**, *33*, 491.

Table II. Intramolecular Distances of **7a**·(C_7H_8)·1.25(CH_2Cl_2) Involving the Non-Hydrogen Atoms[a]

Sn1–S1	2.595 (1)	N2–C8	1.364 (5)
Sn1–S2	2.581 (1)	N3–C1	1.319 (5)
Sn1–N3	2.318 (3)	N3–C5	1.314 (5)
Sn1–C9	2.204 (5)	N4–C4	1.324 (5)
Sn1–C17	2.199 (4)	N4–C8	1.327 (5)
Sn2–S3	2.592 (1)	C1–C2	1.451 (6)
Sn2–S4	2.582 (1)	C2–C3	1.382 (6)
Sn2–N4	2.305 (3)	C3–C4	1.450 (6)
Sn2–C13	2.196 (5)	C5–C6	1.447 (6)
Sn2–C21	2.198 (4)	C6–C7	1.364 (6)
Ni–N1	1.871 (3)	C7–C8	1.448 (6)
Ni–N1	1.871 (3)	C9–C10	1.529 (7)
Ni–N2	1.873 (4)	C9–C11	1.507 (7)
Ni–N2	1.873 (4)	C9–C12	1.513 (7)
S1–C2	1.731 (4)	C13–C14	1.465 (8)
S2–C6	1.733 (4)	C13–C15	1.530 (9)
S3–C7	1.726 (4)	C13–C16	1.468 (8)
S4–C3	1.718 (4)	C17–C18	1.520 (7)
N1–C1	1.360 (5)	C17–C19	1.507 (8)
N1–C4	1.366 (5)	C17–C20	1.507 (7)
		C21–C22	1.517 (7)
		C21–C23	1.511 (7)
		C21–C24	1.514 (8)

[a] Distances are in angstroms. Estimated standard deviations in the least significant figure are given in parentheses.

Table III. Intramolecular Bond Angles for **7a**·(C_7H_8)·1.25(CH_2Cl_2) Involving the Non-Hydrogen Atoms[a]

S1–Sn1–S2	143.49 (4)	S1–C2–C3	133.1 (3)
S1–Sn1–N3	76.54 (9)	C1–C2–C3	105.9 (4)
S1–Sn1–C9	103.3 (1)	S4–C3–C2	133.5 (3)
S1–Sn1–C17	92.1 (1)	S4–C3–C4	121.6 (3)
S2–Sn1–N3	76.76 (9)	C2–C3–C4	104.9 (4)
S2–Sn1–C9	103.2 (1)	N1–C4–N4	126.0 (4)
S2–Sn1–C17	94.1 (1)	N1–C4–C3	112.7 (4)
N3–Sn1–C9	94.5 (2)	N4–C4–C3	121.2 (4)
N3–Sn1–C17	142.5 (2)	N2–C5–N3	125.8 (4)
C9–Sn1–C17	123.0 (2)	N2–C5–C6	112.1 (4)
S3–Sn2–S4	147.12 (4)	N3–C5–C6	122.1 (4)
S3–Sn2–N4	77.16 (9)	S2–C6–C5	120.5 (3)
S3–Sn2–C13	101.7 (1)	S2–C6–C7	133.5 (3)
S3–Sn2–C21	92.2 (1)	C5–C6–C7	106.0 (4)
S4–Sn2–N4	77.21 (9)	S3–C7–C6	133.4 (3)
S4–Sn2–C13	101.9 (1)	S3–C7–C8	121.0 (3)
S4–Sn2–C21	94.3 (1)	C6–C7–C8	105.6 (4)
N4–Sn2–C13	97.9 (2)	N2–C8–N4	125.3 (4)
N4–Sn2–C21	139.9 (2)	N2–C8–C7	112.6 (3)
C13–Sn2–C21	122.2 (2)	N4–C8–C7	122.1 (4)
N1–Ni–N1	180.00	Sn1–C9–C10	109.3 (3)
N1–Ni–N2	89.8 (1)	Sn1–C9–C11	109.6 (3)
N1–Ni–N2	90.2 (1)	Sn1–C9–C12	107.5 (4)
N2–Ni–N2	180.00	C10–C9–C11	109.5 (5)
Sn1–S1–C2	98.1 (1)	C10–C9–C12	109.4 (5)
Sn1–S2–C6	97.4 (1)	C11–C9–C12	111.5 (5)
Sn2–S3–C7	98.2 (1)	Sn2–C13–C14	110.0 (4)
Sn2–S4–C3	97.1 (1)	Sn2–C13–C15	108.7 (4)
Ni–N1–C1	127.6 (3)	Sn2–C13–C16	109.3 (4)
Ni–N1–C4	128.0 (3)	C14–C13–C15	108.2 (7)
C1–N1–C4	104.4 (3)	C14–C13–C16	114.8 (8)
Ni–N2–C5	127.6 (3)	C15–C13–C16	105.7 (8)
Ni–N2–C8	128.6 (3)	Sn1–C17–C18	108.7 (3)
C5–N2–C8	103.7 (3)	Sn1–C17–C19	108.8 (3)
Sn1–N3–C1	118.4 (3)	Sn1–C17–C20	109.0 (3)
Sn1–N3–C5	116.9 (3)	C18–C17–C19	110.8 (5)
C1–N3–C5	122.3 (4)	C18–C17–C20	109.9 (5)
Sn2–N4–C4	117.7 (3)	C19–C17–C20	109.7 (5)
Sn2–N4–C8	118.2 (3)	Sn2–C21–C22	107.8 (3)
C4–N4–C8	122.2 (4)	Sn2–C21–C23	107.6 (3)
N1–C1–N3	126.5 (4)	Sn2–C21–C24	109.4 (3)
N1–C1–C2	112.1 (4)	C22–C21–C23	109.7 (4)
N3–C1–C2	121.4 (4)	C22–C21–C24	111.0 (4)
S1–C2–C1	121.0 (3)	C23–C21–C24	111.2 (5)

[a] Angles are in degrees, esd in the least significant figure are given in parentheses.

Table IV. Crystallographic Data for Mg(omtp)(H_2O) (**3b**·H_2O)

molecular formula	$C_{24}H_{24}MgN_8S_8 \cdot H_2O$
formula weight, amu	723.31
crystal system	orthorhombic
space group	*Pnma*
a, Å	14.279 (3)
b, Å	26.403 (6)
c, Å	8.257 (2)
V, Å^3	3113 (1)
Z	4
temperature, °C	−84
F(000)	1488
ρ(calcd), g/cm^3	1.55
crystal dimns, mm	0.22 × 0.28 × 0.28
radiation	Mo Kα (λ = 0.7107 Å)
μ, cm^{-1}	6.1
scan type	$\theta/2\theta$
2θ range, deg	$4 \le 2\theta \le 50$
total no. of reflcns	3158
no. of unique obsd reflcns	2407 ($F_o \ge 5\sigma(F_o)$)
no. of least-squares parameters	220
R	0.089
R_w	0.133

Table V. Bond Lengths for Mg(omtp)(H_2O) (**3b**·H_2O)[a]

S1–C2	1.745 (7)	N1–C4	1.365 (8)
S1–C9	1.802 (9)	N2–C5	1.345 (8)
S2–C3	1.764 (6)	N2–C8	1.380 (8)
S2–C10a	1.727 (14)	N3–C1	1.314 (7)
S2–C10b	1.891 (15)	N4–C4	1.343 (8)
S3–C6	1.718 (7)	N4–C5	1.336 (8)
S3–C11a	1.808 (15)	N5–C8	1.324 (7)
S3–C11b	1.773 (18)	C1–C2	1.466 (9)
S4–C7	1.736 (7)	C2–C3	1.343 (9)
S4–C12	1.760 (12)	C3–C4	1.458 (8)
Mg–O	2.028 (7)	C5–C6	1.476 (8)
Mg–N1	2.026 (8)	C6–C7	1.378 (9)
Mg–N2	2.045 (5)	C7–C8	1.474 (9)
N1–C1	1.373 (8)		

[a] Distances are in angstroms. Estimated standard deviations in the least significant figure are given in parentheses.

as such. In addition, each CH_2Cl_2 was modeled as having two rotational orientations. A CH_2Cl_2 occupancy factor of 0.6 gave the best isotropic refinement, and this was in agreement with occupancy values of 0.625 from elemental analysis and 0.65 from crystal density measurements. Table I gives the pertinent crystallographic parameters and Tables II and III give the bond lengths and angles, respectively. Fractional coordinates, anisotropic thermal parameters, and structure factors appear in the supplementary material.

The single-crystal X-ray diffraction data of Mg(omtp)(H_2O) (**3b**·H_2O) were collected at Colorado State University using a Nicolet *R3m* diffractometer. The unit cell constants were obtained from a least-squares fit of setting angles for 25 reflections ($2\theta_{av}$ = 22.32°). Lorentz and polarization corrections were applied; no absorption correction was applied due to the low absorption coefficient. The structure was solved in *Pnma* by use of direct methods (SOLV) and the hydrogen atoms were included in idealized positions (C–H = 0.96 Å, U(H) = 1.2 × U_{iso}(C)); non-hydrogen atoms were refined with anisotropic thermal parameters. **3b**·H_2O is positioned about a mirror plane with Mg, O, N3, and N5 on the symmetry element. Disorder/high thermal motion was encountered with three of the methyl carbon atoms: C10, C11, and C12. Two orientations of the methyl groups for both C10 and C11 were located and refined (occupancy factor 0.50 (2) and 0.50 (2) for C10a and C10b, respectively, and 0.45 (1) and 0.55 (1) for C11a and C11b, respectively; occupancy factors for C10a, C10b, C11a, and C11b were set at 0.50 during final refinement, with H atoms not included for these C atoms); although only one position for C12 was indicated, C12 exhibited a significantly higher equivalent isotropic thermal parameter than other atoms. Several observed reflections (with extremely broad profiles) violated the extinction conditions required for the *n* glide. Neutral atom scattering factors and anomalous dispersion corrections were used;[11a] all calculations were performed using the SHELX<<tL[11b] program library. Table IV gives the pertinent crystallographic parameters, and Tables V and VI give the bond lengths and angles, respectively. Fractional coordinates, anisotropic thermal parameters and structure factors appear in the supplementary material.

(11) (a) *International Tables for X-ray Crystallography*; Wiley: New York, 1974; Vol. IV. (b) Sheldrick, G. M. *SHELXTL*, Rev. 5.1; Nicolet XRD Corp.: Madison, Wisconsin, 1985.

Table VI. Bond Angles for Mg(omtp)(H_2O) (**3b**·H_2O)[a]

C2–S1–C9	103.0 (3)	N1–C1–C2	108.8 (5)
C3–S2–C10a	107.8 (5)	N3–C1–C2	124.0 (6)
C3–S2–C10b	102.5 (6)	S1–C2–C1	120.5 (5)
C6–S3–C11a	104.4 (6)	S1–C2–C3	132.3 (5)
C6–S3–C11b	109.4 (6)	C1–C2–C3	107.2 (5)
C7–S4–C12	101.7 (4)	S2–C3–C2	129.9 (5)
O–Mg–N1	106.5 (2)	S2–C3–C4	123.0 (5)
O–Mg–N2	105.2 (2)	C2–C3–C4	107.2 (5)
N1–Mg–N2	85.5 (2)	N1–C4–N4	127.2 (5)
N1–Mg–N1′	85.2 (3)	N1–C4–C3	109.4 (5)
N1–Mg–N2′	148.4 (2)	N4–C4–C3	123.2 (6)
N2–Mg–N2′	86.7 (3)	N2–C5–N4	127.0 (6)
Mg–N1–C1	126.2 (4)	N2–C5–C6	110.3 (5)
Mg–N1–C4	125.2 (4)	N4–C5–C6	122.8 (5)
C1–N1–C4	107.3 (5)	S3–C6–C5	130.2 (5)
Mg–N2–C5	126.7 (4)	S3–C6–C7	123.9 (5)
Mg–N2–C8	124.3 (4)	C5–C6–C7	105.9 (5)
C5–N2–C8	108.2 (5)	S4–C7–C6	128.2 (5)
C1–N3–C1′	123.5 (8)	S4–C7–C8	125.0 (5)
C4–N4–C5	123.1 (6)	C6–C7–C8	106.8 (5)
C8–N5–C8′	123.8 (8)	N2–C8–N5	127.9 (6)
N1–C1–N3	127.2 (6)	N2–C8–C7	108.7 (5)
		N5–C8–C7	123.3 (6)

[a] Angles in degrees, esd in the least significant figure are given in parentheses.

Synthetic Details. Bis(benzylthio)maleonitrile (2). This compound was reported previously without synthetic details.[12] A solution of benzyl bromide (52 mL, 218 mmol) in methanol (100 mL) was added dropwise to a solution of Na_2mnt (20.2 g, 109 mmol) in methanol (150 mL) at 0 °C. Yellow solid precipitated from the reaction mixture. The precipitate was filtered and washed thoroughly with 1:1 MeOH–H_2O (to remove NaBr) and then with hexane (to remove unreacted benzyl bromide) and dried in vacuo. Yield 22.0 g (60%). Yellow needles, mp 69.5–70.5 °C (lit. mp 68–69 °C). ^{1}H NMR ($CDCl_3$) δ 7.35 (m, 5 H), 4.27 (s, 2 H).

[2,3,7,8,12,13,17,18-Octakis(benzylthio)porphyrazinato]magnesium(II) (Mg(obtp), 3a). Magnesium metal (0.60 g, 25 mmol) was placed in a nitrogen-filled flask and heated to ca. 500 °C with a bunsen flame. The flask was cooled and 1-propanol (200 mL) was introduced. A small chip of I_2 was added and the mixture was heated to reflux for 16 h to form a magnesium propoxide suspension. Dinitrile **2** (16.0 g, 50 mmol) was added and the mixture was heated to reflux for another 12 h, turning dark blue. The reaction mixture was cooled slowly to 25 °C and then to 5 °C overnight. The dark precipitate was collected by suction filtration and washed with several portions of 1% HCl in EtOH. The dark blue solid was vacuum dried to give 15 g of crude product. The solid was purified as follows. A 4-g aliquot was dissolved in EtOH-free chloroform (250 mL) and silica gel (100 mL) was added. The blue pigment adsorbed to the silica, and the silica was filtered off and washed with $CHCl_3$ until the filtrate was colorless. The silica was slurried with 5% MeOH in $CHCl_3$ (250 mL) and then filtered. The blue filtrate was rotary evaporated to a blue oil and then vacuum dried. The resulting solid was chromatographed on silica gel using 20:1 $CHCl_3$–Et_2O, and the major, navy-blue component was collected, rotary evaporated to dryness, and recrystallized from acetone–heptane. Overall yield 35–40%, as the monoacetone adduct. Anal. ($C_{72}H_{56}MgN_8S_8 \cdot C_3H_6O$): obsd (calcd) C, 65.01 (65.65); H, 4.67 (4.55); N, 7.94 (8.17); S, 18.57 (18.69). Shiny blue plates, mp 111–113 °C. ^{1}H NMR (d^6-acetone) δ 7.35 (m, 16 H), 7.05 (m, 24 H), 5.26 (s, 16 H). UV–vis ($CHCl_3$) λ_{max} (log ϵ) 382 (4.84), 500 (4.11), 680 nm (4.87).

2,3,7,8,12,13,17,18-Octakis(benzylthio)porphyrazine (H_2(obtp), 4). Compound **3a** (2.0 g, 1.5 mmol) was dissolved in excess trifluoroacetic acid (30 mL), stoppered, and stored in the dark for 16 h. The black slurry was poured into ice water (ca. 400 mL) and stirred. The suspension was neutralized with aqueous KOH, and the solid was collected by filtration and washed thoroughly with portions of water, MeOH, and Et_2O. Recrystallization from hot chlorobenzene afforded 1.8 g of crystalline product after vacuum drying (90% yield). Anal. ($C_{72}H_{58}N_8S_8$): obsd (calcd) C, 66.98 (66.95); H, 4.45 (4.53); N, 8.73 (8.67); S, 20.07 (19.85). Long green fibers, mp >250 °C dec. ^{1}H NMR ($CDCl_3$) δ 7.35 (m, 16 H), 7.10 (m, 24 H), 5.19 (s, 16 H), −1.72 (s, 2 H). UV–vis

(12) Wolf, W.; Degener, E.; Petersen, S. *Angew. Chem.* **1960**, *72*, 963–966.

(PhCl): λ_{max} (log ϵ) 354 (4.63), 508 (4.30), 648 (4.41), 716 nm (4.54). FAB-MS: 1291 ($M + H^+$).

[2,3,7,8,12,13,17,18-Octakis(benzylthio)porphyrazinato]nickel(II) (Ni(obtp), 5a). Metal-free **4** (1.50 g, 1.16 mmol), anhydrous $Ni(OAc)_2$ (1.7 g, 10-fold excess), chlorobenzene (40 mL), and DMF (15 mL) were heated to reflux under nitrogen for 5 h. Progress of the reaction was monitored by optical spectra of aliquots of the reaction mixture diluted in chlorobenzene. The solution was brought slowly back to 25 °C, and the precipitate was filtered off and washed with 5% HCl in MeOH, MeOH, and acetone. The remaining black crystals were vacuum dried, yielding 1.48 g (95%). Anal. ($C_{72}H_{56}N_8NiS_8$): obsd (calcd) C, 64.33 (64.13); H, 4.19 (4.19); N, 8.33 (8.31); S, 19.21 (19.02). Shiny black needles, mp >250 °C dec. ^1H NMR ($CDCl_3$) δ 7.31 (m, 16 H), 7.11 (m, 24 H), 5.12 (s, 16 H). UV–vis (PhCl): λ_{max} (log ϵ) 330 (4.60), 490 (4.27), 672 nm (4.63).

[2,3,7,8,12,13,17,18-Octakis(benzylthio)porphyrazinato]copper(II) (Cu(obtp), 5b). Bis(acetato)diamminecopper(II)[13] (2.00 g, 12.8 mmol) and chlorobenzene (50 mL) were heated to reflux under N_2 for 2 h to produce a very fine copper(II) acetate suspension. Metal-free **4** was added and reflux was continued for another 4 h. The solution was slowly cooled to 25 °C and then 5 °C overnight, and the precipitate was filtered off, washed with dilute aqueous HCl and methanol until the washings were colorless, and dried in vacuo. Yield 1.17 g (70%) black needles. Anal. ($C_{72}H_{56}CuN_8S_8$): obsd (calcd) C, 64.15 (63.90); H, 4.45 (4.17); N, 8.83 (8.28); S, 18.57 (18.95). UV–vis (PhCl): λ_{max} (log ϵ) 356 (4.63), 502 (4.28), 620 sh (4.44), 673 nm (4.86).

Octasodium (Porphyrazine-2,3,7,8,12,13,17,18-octathiolato)nickelate(II) (Na_8-*star*-Ni(pzS_8), 6a). Schlenk techniques were used in this step. Ni(obtp) (1.348 g, 1.00 mmol) was suspended in a solution of liquid NH_3 (250 mL) and THF (50 mL) at −78 °C. Sodium metal (0.60 g, 26.1 mmol) was freshly cut under THF and added in small pieces. The solution was allowed to reflux at −33 °C for 30 min, whereupon the solution turned reddish-purple and then green. Ammonium nitrate (1.30 g, 16.2 mmol) was cautiously added to neutralize the excess sodium and sodium amide. *Caution! Addition must be slow because NH_3 gas evolves rapidly!* The ammonia was vented off under a stream of nitrogen and the THF was removed in vacuo. This yielded a fine purple powder which was a mixture of sodium nitrate and the sodium salt of the octathiolate. The solid is quite air-sensitive, and no attempt was made to determine the yield. However, the debenzylation step is essentially quantitative as no benzylic resonances were observed in the ^1H NMR spectra of subsequent derivatized compounds.

μ-[(Porphyrazine-2,3,7,8,12,13,17,18-octathiolato)nickel(II)-(*S*,*N*,*S*)^4]tetrakis(di-*tert*-butyltin(IV)) (7a). Ni(obtp) (1.348 g, 1.00 mmol) was deprotected by the method above. The resulting octathiolate was dissolved in deaerated water (100 mL) and methanol (50 mL). To this was added dropwise a filtered, degassed solution of di-*tert*-butyltin dinitrate in MeOH (50 mL), formed from the metathesis of $(t\text{-Bu})_2SnCl_2$ (1.33 g 4.37 mmol) and $AgNO_3$ (1.38 g, 8.12 mmol). The violet solution turned blue and a precipitate formed. The solution was stirred for 30 min and then filtered under ambient conditions. The solid was washed with methanol until washings were colorless. The solid was then dissolved in hot toluene, dried over $MgSO_4$, filtered, and taken to near dryness on a rotary evaporator. The microcrystalline solid was collected by filtration and washed with *n*-hexane until washings were pale green. The green solid was dried in vacuo to give 0.58 g of product (37% yield). Analytically pure material was obtained by recrystallization from CH_2Cl_2–toluene. Anal. ($C_{48}H_{72}N_8NiS_8Sn_4 \cdot C_7H_8 \cdot 1.25(CH_2Cl_2)$): obsd (calcd) C, 38.79 (38.62); H, 4.73 (4.72); N, 6.37 (6.40); S, 14.45 (14.66); Cl, 5.07 (5.07). Greenish-black prisms or green fibers, mp >250 °C dec. ^1H NMR ($CDCl_3$) δ 1.48 s. ^{119}Sn NMR ($CDCl_3$, $SnMe_4$ external reference) δ 4.50 (s). UV–vis (1,2-dichloroethane): λ_{max} (log ϵ) 260 (4.65), 304 (4.30), 336 (3.96), 438 (3.97), 516 sh, 676 nm (4.73).

μ-[(Porphyrazine-2,3,7,8,12,13,17,18-octathiolato)nickel(II)-(*S*,*N*,*S*)^4]tetrakis(di-*n*-butyltin(IV)) (7b). This was prepared by an analogous procedure to that used for the di-*tert*-butyltin(V) derivative, except that di-*n*-butyltin(IV) dichloride was used and the solid precipitate was extracted with hot cyclohexane rather than toluene. The product was isolated as a purple amorphous solid in ca. 80% yield, based on starting Ni(obtp) (**3**). Anal. ($C_{48}H_{72}N_8NiS_8Sn_4$): obsd (calcd) C, 37.66 (37.17); H, 470 (4.68); N, 6.74 (7.22). ^1H NMR ($CDCl_3$) δ 0.93 t, 1.39 q, 1.48 m, 1.68 m. ^{119}Sn NMR ($CDCl_3$, $SnMe_4$ external reference): δ 20.7 s. UV–vis (cyclohexane): λ_{max} (log ϵ) 284 sh (4.20), 342 (3.97), 414 (3.96), 650 nm (4.73). UV–vis (1,2-dichloroethane): λ_{max} (log ϵ) 284 (4.20), 332 (3.97), 412 (3.96), 675 nm (4.81).

μ-[(Porphyrazine-2,3,7,8,12,13,17,18-octathiolato)copper(II)-(*S*,*N*,*S*)^4]tetrakis(di-*tert*-butyltin(IV)) (8). Using Schlenk techniques, Cu(obtp) (0.241 g, 0.18 mmol) was suspended in a solution of liquid NH_3 (100 mL) and THF (10 mL) at −78 °C. Sodium metal (0.114 g, 4.96 mmol) was freshly cut under THF and added in small pieces. The solution was allowed to reflux at −33 °C for 30 min, whereupon the solution turned violet-blue, then reddish-purple, and then green. Ammonium nitrate (0.252 g, 3.15 mmol) was cautiously added to a neutralize the excess sodium and sodium amide. *Caution! Addition must be slow because NH_3 gas evolves rapidly!* The ammonia was vented off under a stream of nitrogen and the THF was removed in vacuo. This yielded a fine purple powder which was a mixture of sodium nitrate and the sodium salt of the octathiolate. The resulting octathiolate was dissolved in deaerated water (50 mL) and methanol (40 mL). To this was added dropwise a filtered, degassed solution of di-*tert*-butyltin dinitrate in MeOH (50 mL), formed from the metathesis of $(t\text{-Bu})_2SnCl_2$ (0.260 g, 0.86 mmol) and $AgNO_3$ (0.254 g, 1.5 mmol). The blue-violet solution turned greenish-blue and a dark precipitate formed. The solution was stirred for 30 min and then filtered under ambient conditions. The solid was washed with methanol until washings were colorless. The solid was then dissolved in hot benzene, dried over $MgSO_4$, filtered, and taken to near dryness on a rotary evaporator. The microcrystalline solid was collected by filtration and washed with hexane until washings were pale green. The green solid was dried in vacuo to give 0.120 g of product (41% yield). Anal. ($C_{48}H_{72}CuN_8S_8Sn_4 \cdot C_6H_6$): obsd (calcd) C, 40.33 (39.69); H, 4.89 (4.81); N, 6.97 (6.86); S, 15.69 (15.70). UV–vis (1,2-dichloroethane): λ_{max} (log ϵ) 256 (4.75), 308 (4.45), 424 (4.13), 690 nm (4.81).

Results and Discussion

Synthesis of the *star*-Porphyrazine Complexes. Our entry-point into the *star*-porphyrazine–S_8 system is the dithiolene ligand maleonitriledithiolato (mnt^{2-}) (**1**, Scheme I). This cannot be cyclized directly to form the desired porphyrazine, but alkylation of the thiolate groups gives a dicyano compound that is readily cyclized by the magnesium alkoxide method introduced by Linstead.[14] Octakis(alkylthio)porphyrazines **3** with R = Me,[9,15] *t*-Bu,[16] $PhCH_2$[7] and 2R = $-CH_2CH_2-$[12] and $-CH(Ph)CH_2-$[17] have been synthesized in this way. The present study involves complexes **3a** and **3b**. The benzyl and methyl groups were attractive candidates because they are among the few thiolate protecting groups which are robust enough to endure the subsequent harsh reaction conditions.[18] Complete dealkylation of the methyl-protected macrocycles was unsuccessful,[19] so our efforts to prepare porphyrazineoctathiolate **6** focussed on the benzyl-protected macrocycle, which can be dealkylated completely.

The thin-layer chromatographs of the crude magnesium–porphyrazine complexes **3a** and **3b** suggest that they also contain other porphyrazine-like byproducts; these have not been characterized. In the case of **3a**, the two-stage chromatographic process yields the pure material as the crystalline monoacetone adduct in approximately 35–40% yield. The magnesium atom is easily removed using neat CF_3COOH to give **4**, and substitution with nickel or copper to give **5a** and **5b** proceeds smoothly using standard high-temperature metalation procedures.[20] Complete removal of the benzyl groups is achieved by using sodium metal reduction in liquid ammonia. The resulting octathiolate **6** is very air-sensitive, even in the solid state, and must be manipulated using Schlenk techniques. The octathiolate **6** dissolves in water or aqueous alcohols to give a brilliant purple solution that may be subsequently treated with "capping" reagents to give air-stable pentametallic *star*-porphyrazine complexes. The use of dialkyltin(IV) dinitrate gives the dialkyltin(IV)-capped Ni or Cu

(13) Bernard, M. A.; Busnot, F. *Bull. Soc. Chim. Fr.* **1969**, 3061–3064.

(14) Linstead, R. P.; Whalley, M. *J. Chem. Soc.* **1952**, 4839–4846.

(15) (a) Bottomley, L. A.; Chiou, W. J. H. *J. Electroanal. Chem.* **1986**, *198*, 331–346. (b) Qin, Z.; Peng, Z.; Yang, M.; Liu, J.; Long, D.; Chen, X. *Wuhan Daxue Xuebao, Ziran Kexueban* **1985**, 65–71. (c) Komarov, R. D.; Lebedeva, G. A. *Soversh. Protsessov. Krasheniya Metodov Sint. Krasitelei* **1983**, *59–60*, 41–47.

(16) Kopranenkov, V. N.; Goncharova, L. S.; Luk'yanets, E. A. *J. Org. Chem. USSR* **1979**, *15*, 1076.

(17) Hahn, W. E.; Kujawski, A. *Soc. Sci. Lodz, Acta Chim.* **1971**, *16*, 129–136.

(18) (a) Greene, T. In *Protective Groups in Organic Chemistry*; John Wiley and Sons, Inc.: New York, 1981; Chapter 6. (b) Hiskey, R. G.; Rao, V. R.; Rhodes, W. G. In *Protective Groups in Organic Chemistry*; McOrmie, J. F. W., Ed.; Plenum Publ. Co. Ltd.: London, 1973; Chapter 6.

(19) Van Wallendael, S. E. Unpublished results.

(20) Buchler, J. W. In *The Porphyrins*; Dolpin, D., Ed.; Academic Press: New York, 1978; Vol. 1, Chapter 10.

Scheme I[a]

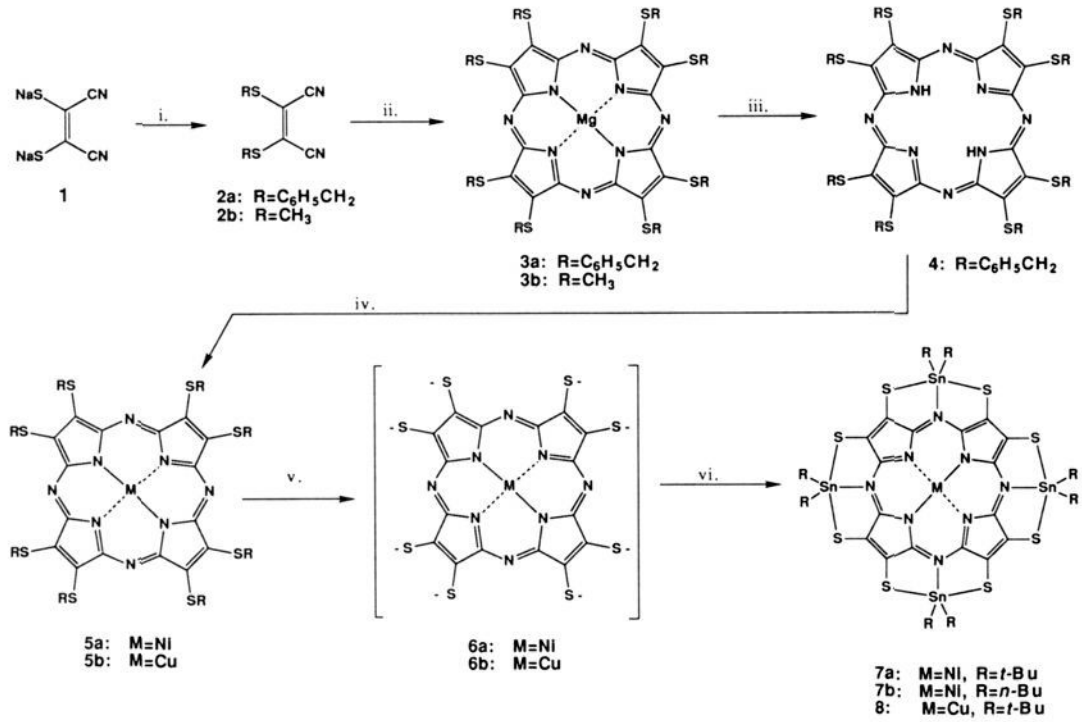

[a] (i) RX = $PhCH_2Br$ or CH_3I/MeOH; (ii) $Mg(OPr)_2$, PrOH, 100 °C; (iii) CF_3CO_2H, 25 °C; (iv) $M(OAc)_2$, PhCl, 140 °C; (v) Na, NH_3, THF, −33 °C; (vi) $R_2Sn(NO_3)_2$, H_2O, 25 °C.

macrocycle in acceptable yields (R = *n*-Bu, 79% for **7b**, purple amorphous solid; R = *t*-Bu, 37% for **7a**, M = Ni; 41% for **8**, M = Cu, green crystalline solid, based on **5**). The alternative use of dialkyltin(IV) dichlorides results in a significant reduction in yield; this may be in part due to the propensity for the chloride ion to coordinate to tin (vide infra).

X-ray Crystal Structure of 7a. The pertinent parameters for the data collection and structure determination of **7a** are compiled in Table I. *star*-Porphyrazine **7a** crystallizes in the monoclinic space group *C*2/*c* (No. 15) with four macrocycles and four ordered toluene molecules per unit cell. The planar macrocyclic molecules form linear stacks along the *z*-axis, with the macrocycles being separated by interleaving toluene molecules. The central nickel atom of the macrocycle rests on an inversion center, and the three collinear carbon atoms of the toluene molecule lie on a 2-fold rotation axis. Between the chains there are open linear channels, and poorly ordered dichloromethane molecules occupy these channels.

Figure 2 shows the molecular structure of **7a**. The porphyrazine and the eight sulfur atoms are very nearly planar, with the maximum deviation from the least-squares plane being only 0.10 (1) Å for S(4). The tin atoms are coordinated by the porphyrazineoctathiolato in a tridentate (S–N–S) fashion. The two adjacent independent ("cis") tin atoms lie above the least-squares plane of the ligand by 0.73 (1) and 0.54 (1) Å; the other two, which are related by the inversion center at Ni, lie below, in a pseudochair arrangement. The coordination geometry around the tin atoms is distorted square pyramidal, with one *tert*-butyl group at the apex and the other occupying the fourth basal position.

Tables II and III contain the bond distances and bond angles for the non-hydrogen atoms of the *star*-porphyrazine complex. To our knowledge, there have been no reported crystal structures of diorganyltin(IV) complexes bearing a tridentate (S–N–S) chelating ligand, although the structure of $Ph_2Sn(sat)$ has been reported, where $(sat)^{2-}$ is a tridentate (S–N–O) chelating ligand.[21] The Sn–S and Sn–N bonds of **7a** are slightly elongated with

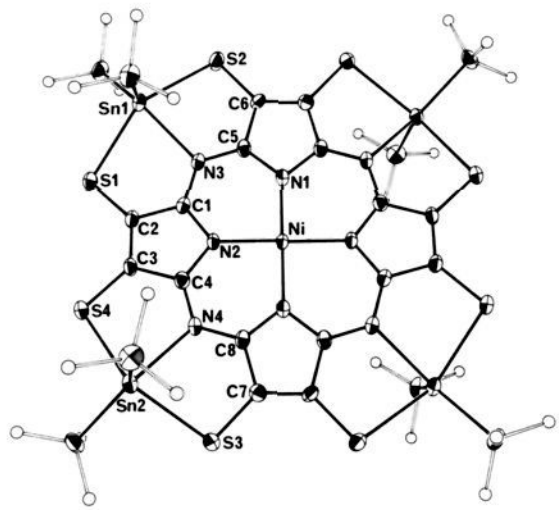

Figure 2. ORTEP diagram of **7a**. For clarity, the hydrogen atoms have been omitted and the methyl carbons have been drawn arbitrarily small.

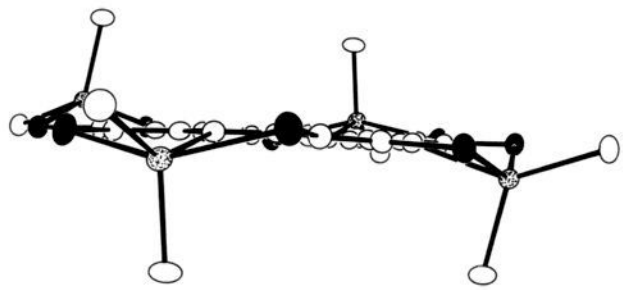

Figure 3. ORTEP diagram of **7a**, emphasizing the planarity of the porphyrazineoctathiolato ligand. Sulfur atoms are drawn in black and tin atoms are shaded. Methyl groups are omitted for clarity.

averages of 2.588 (1) and 2.311 (3) Å, respectively, as compared to 2.496 and 2.217 Å as seen in $Ph_2Sn(sat)$. The S–Sn–N bond

(21) Preut, H.; Haupt, H.-J.; Huber, F.; Cefalú, R.; Barbieri, R. *Z. Anorg. Allg. Chem.* **1974**, *407*, 257.

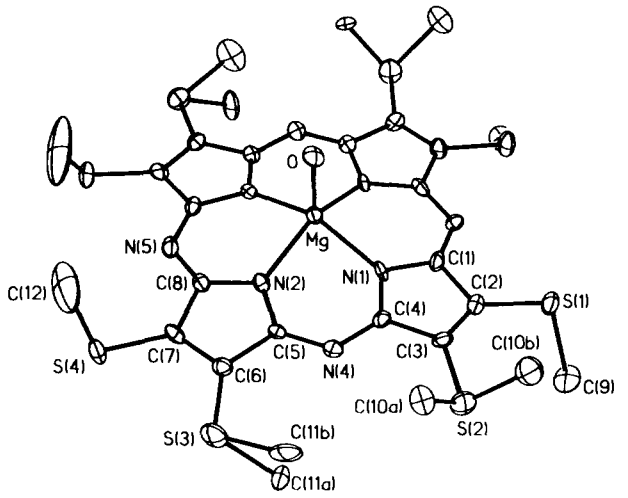

Figure 4. ORTEP diagram of **3b**·H_2O with hydrogen atoms omitted for clarity. The disorder in C10 and C11 is modeled using two sites (a and b) for each atom.

angles in both **7a** and Ph_2Sn(sat) are acute, ranging from 76.76 (9)° to 77.21 (9)° in **7a** to 78.2 (1)° as seen in Ph_2Sn(sat). The Sn–C distances are typical for diorganyltin complexes, averaging 2.200 (5) Å; these values can range from 2.12 to 2.24 Å.[21]

X-ray Crystal Structure of Mg(omtp)(H_2O) (3b·H_2O). To ascertain the structural consequences of tridentate (S–N–S) coordination on the porphyrazineoctathiolato ligand, we undertook a crystallographic study of a representative octakis(alkylthio)porphyrazine. The M(obtp) complexes crystallize with a fiber-like habit that is unsuitable for single-crystal X-ray diffraction. However, adequate single crystals of Mg(omtp) were obtained as the monohydrate Mg(omtp)(H_2O) (**3b**·H_2O) and the crystal structure was determined. This compound crystallizes in the orthorhombic space group *Pnma* with four macrocycles per unit cell. A mirror plane bisects the molecule and contains *meso*-nitrogens N(3) and N(5), the central Mg atom, and the oxygen atom of the axially coordinated H_2O molecule. Two methyl carbons (C10 and C11) show disorder in that two orientations (*a* and *b*) were refined and the thermal parameters for C12 are large (supplementary material); thus the structure could only be refined to a residual value of $R = 0.089$. However, the anisotropic thermal parameters for the porphyrazineoctathiolate core of the molecule are acceptably low and definite conclusions can be drawn about this portion of the macrocycle.

The bond distances and angles for **3b**·(H_2O) are given in Tables V and VI. The five-coordinate magnesium atom is displaced 0.555 (3) Å above the plane of the four pyrrole nitrogen atoms. This is significantly higher than the M–Ct displacement distance of 0.496 Å for Mg(pc)(H_2O).[22a] These two porphyrazine M–Ct distances are longer than those of five-coordinate magnesium porphyrins: 0.414 Å for Mg(tpp)(dipicoline),[22b] 0.450 for Mg(tpp)(H_2O)·acetone,[22c] and 0.273 Å for Mg(tpp)(H_2O).[22d] This is consistent with the picture of a smaller central hole in the porphyrazines. The porphyrazineoctathiolate core (defined from the best-fit plane: C1 to C8 and S1 to S4) is essentially planar with the largest deviation from the plane being only 0.255 (2) Å for S3. There appears to be some variation in bond lengths and angles for positions that are symmetry~related in an idealized D_{4h} macrocycle. For instance, the C_β–S distances vary from 1.718 (7) to 1.764 (6) Å, the C_β–C_β distances are 1.343 (9) and 1.378 (9) Å, and the C_β–C_β–S angles range from 123.9 (5)° to 132.3 (5)°.

Structural Comparison of the Porphyrazines and Phthalocyanines. Although porphyrazines have been known for over 50 years,[23] other than phthalocyanines there have been no reported porphyrazine crystal structures.[24] Therefore, it is of interest to compare the planar porphyrazine cores of **3b** and **7a** with those of metallophthalocyanine M(pc) complexes. For comparison, the symmetry-averaged bond angles and distances for the sulfur atoms, α- and β-carbon atoms, and meso and pyrrole nitrogen atoms of Mg(omtp)(H_2O) [**3b**·(H_2O)] and [(*t*-Bu)$_2$Sn]$_4$-*star*-Ni(pz)S_8 [**7a**] are presented in Table VII. Also included are the mean bond distances and angles typical for M(pc) complexes.

Table VII. Symmetry Averaged Bond Distances and Angles for Porphyrazine and Phthalocyanine Macrocycles

	7a	**3b**·H_2O	M(pc)[a]
	Bond Distances (Å)[b]		
C_α–N_p	1.366 (5)	1.367 (14)	1.376
C_α–C_β	1.449 (2)	1.469 (8)	1.453
C_β–C_β	1.373 (13)	1.361 (25)	1.395
C_α–N_m	1.321 (6)	1.329 (13)	1.328
C_β–S	1.727 (6)	1.741 (19)	
	Bond Angles[b]		
C_β–C_β–S	133.4 (2)	128.6 (35)	
C_α–C_β–C_β	105.6 (5)	106.8 (6)	106.7
C_α–N_p–C_α	104.1 (5)	107.8 (6)	108.1
N_m–C_α–N_p	125.9 (5)	127.3 (4)	127.7
C_α–N_m–C_α	122.3 (1)	123.5 (4)	123.2
N_p–C_α–C_β	112.4 (3)	109.3 (7)	109.3
C_α–C_β–S	121.0 (5)	124.7 (41)	
N_m–C_α–N_p	121.7 (5)	123.4 (6)	123.0
N_p–M–N_p	90.0 (2)	85.8 (8)	90[c]
N_p–M–N_p'	180[c]	148.4 (0)	180[c]

[a] Averaged for Mg(pc), Zn(pc), Fe(pc), and Mn(pc) structures. See: Schramm, C. J.; Scaringe, R. P.; Stojakovic, D. R.; Hoffman, B. M.; Ibers, J. A.; Marks, T. J. *J. Am. Chem. Soc.* **1980**, *102*, 6702. [b] Number in parentheses is the standard deviation of the values used in the symmetry average. [c] Value is fixed by crystal symmetry.

Mg(omtp) (**3b**) should provide a reasonably unconstrained structural reference for the metrical parameters at the periphery of the sulfur-encircled pz. The porphyrazineoctathiolate core of **3b** approximates to D_{4h} symmetry (Tables V and VI) as seen for M(pc). The bond distances in **3b** are very similar to those in M(pc), although there is a small but significant contraction of the C_β–C_β bond in **3b**, probably due to the electronic influence of the sulfur substituents. Most of the bond angles in **3b** are in good agreement with those of M(pc) as well.

The coordination of the tin atoms to the meso nitrogens of **7a** appears to have a negligible effect on the bond angles and distances of the porphyrazine core, as represented by **3b**, with one possible exception. The core of **7a** is essentially the same as that of Mg(omtp), including the C_β–C_β bond contraction relative to the M(pc) complexes, except that the C_α–N_p–C_α angle of **7a** is contracted by 4° and the N_p–C_α–C_β angle of **7a** is expanded by 3° relative to **3b**. The most obvious source of this difference might be that the magnesium atom of **3b** lies out of the porphyrazine plane, whereas the nickel atom of **7a** lies in-plane; however, the structural parameters for **3b** are much closer to those of those of the square-planar M(pc) complexes (Table VII) than to **7a**.

The geometry of the peripheral thiolate groups relative to the porphyrazine ring system is of key interest to the use of porphyrazineoctathiolato as a multimetal coordinating ligand. In **7a**, the C_β–C_β–S bond angle formed by the two β-carbons of the ring and the peripheral sulfur atoms is unusually large, with a symmetry-averaged value of 133.4 (2)°. In contrast, the symmetry-averaged C_β–C_β–S bond angle of Mg(omtp) (**3b**) is 128.6 (35)°. The difference suggests that this angle has been slightly opened in **7a** to accommodate bonding to the Sn atoms. For comparison, the C=C—S angle found in metal bis(dithiolene) complexes is 120–122°.[25] The differences between Mg(omtp)

(22) (a) Fischer, M. S.; Templeton, D. H.; Zalkin, A.; Calvin, M. *J. Am. Chem. Soc.* **1971**, *93*, 2622. (b) Choon, O. C.; McKee, V.; Rodley, G. A. *Inorg. Chim. Acta* **1986**, *123*, L11. (c) McKee, V.; Rodley, G. A. *Inorg. Chim. Acta* **1988**, *151*, 233. (d) Timkovich, R.; Tulinsky, A. *J. Am. Chem. Soc.* **1969**, *91*, 4430.

(23) (a) Fischer, H.; Endermann, F. *Annalen* **1937**, *531*, 245. (b) Cook, A. H.; Linstead, R. P. *J. Chem. Soc.* **1937**, 929.

(24) Recently the crystal structure of chloroiron(III) octaethylporphyrazine has been determined: Prof. Jeffrey Fitzgerald, U.S. Naval Academy, personal communication, September 1990.

Table VIII. Comparison of Electronic Spectra of Octakis(alkylthio)porphyrazines with Phthalocyanines (pc)[a]

metal		ligand (obtp)	(omtp)[10]	(pc)[27a]	(pz)[27b]
Mg	(Q)	680 (74.1)	672 (75.2)	674 (49.4)	584 (50.3)
		620 (24.7)	620 (26.5)	647 (43.9)	
		500 (12.9)	500 (12.9)	610 (44.5)	536 (41.7)
	(B)	375 (69.2)	382 (68.9)	347 (47.3)	326 (47.9)
"H_2"		716 (34.7)	709 (35.0)	698 (52.1)	
		648 (25.7)	637 (25.5)	665 (51.8)	
				638 (46.2)	617 (47.5)
		508 (19.9)	515 (20.0)	602 (44.3)	545 (46.0)
		354 (42.7)	367 (42.3)	350 (47.4)	333 (47.0)
Ni	(Q)	672 (42.7)	660 (42.2)	671 (51.0)	577 (47.7)
		620 (22.1)	*620* (21.7)	643 (44.7)	
		490 (18.6)	482 (18.6)		530 (41.4)
	(B)	334 (39.8)	347 (39.9)	351 (45.7)	345 (45.0)
Cu	(Q)	673 (72.8)	667 (48.4)	678 (53.4)	578 (49.8)
		620 (27.4)	*610* (19.9)	648 (45.1)	
		502 (19.2)	497 (14.8)	611 (45.6)	531 (41.3)
	(B)	356 (43.5)	363 (36.2)	350 (47.6)	334 (45.7)

[a] Wavelengths in nm, molar extinctions expressed in 10^{-3} ϵ. Values in italics represent shoulders on larger peaks.

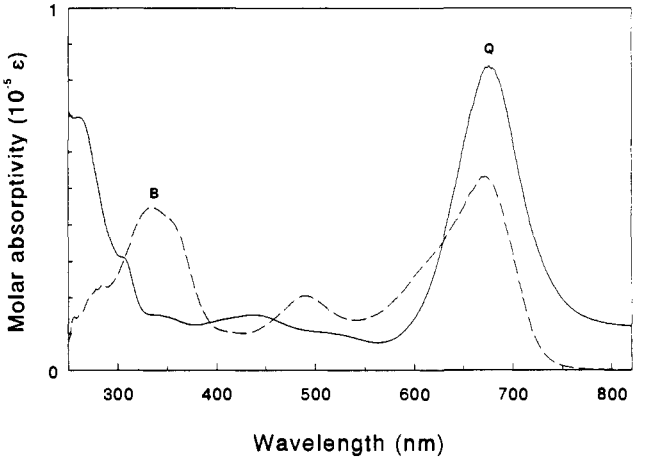

Figure 5. Optical absorption spectra of (---) Ni(obtp) (**5a**) and (—) *star*-porphyrazine (**7a**). Solutions are 20 μM in CH_2Cl_2.

and **7a** suggest that the C–S bonds in **6** should be flexible enough to accommodate bidentate (S–S) coordination as well as tridentate (S–N–S) coordination (Figure 1).

Electronic Absorption Spectroscopy. The electronic absorption maxima of the M(obtp) complexes are tabulated in Table VIII, with the spectrum of **5a** shown in Figure 5. For comparison, the spectral data from the previously reported octakis(methylthio)-porphyrazines, phthalocyanines, and unsubstituted porphyrazines are included. There is a very good qualitative agreement between the benzylthio- and methylthio-substituted macrocycles. The spectra of the Mg, Ni, and Cu derivatives of obtp (**3a**, **5a**, and **5b**) are all quite similar in that as seen in Figure 5 they exhibit a strong low-energy absorbance (Q) at 660–680 nm that is accompanied by a slightly higher energy shoulder at 610–620 nm. For **5a** as well as Ni(omtp), the shoulder is not clearly discernible except for the asymmetric peak shapes. Also present is a less

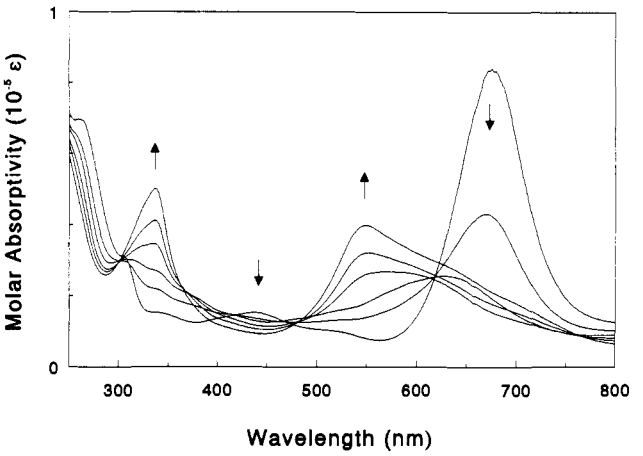

Figure 6. Optical spectra in the presence of Bu_4NF. Solutions contain 20 μM in **7a**, and the plots represent the following F^-/**7a** mole ratios: 0, 1, 2, 4, 6, 8.

intense peak (P) at 500–515 nm and another intense peak (B) at 330–380 nm, also known as the Soret band.[26] The B band also shows marked asymmetry which may be due to overlapping transitions. For the metal-free derivatives the molecular symmetry is reduced from D_{4h} to D_{2h}, and the Q band splits into two distinct peaks as seen for H_2(pc) and free-base porphyrins. The peak positions of the alkylthio-substituted metalloporphyrazines (M = Mg, Ni, Cu) more closely resemble those of the metallophthalocyanines[27a] than their corresponding unsubstituted metalloporphyrazines (Table VIII),[27b] although the peaks are broadened substantially compared to M(pc). This suggests that the sulfur substituents make a significant contribution to the porphyrazine π-electron system.

It is immediately apparent from the electronic spectrum of **7a**, shown in Figure 5, that the coordination of the tin atoms by the meso nitrogen atoms has a profound effect on the electronic structure of the porphyrazine π-system. The absorption maximum at 676 nm is nearly twice as intense as the Q band of the precursor Ni(obtp) (**5a**). The intense band of **5a** found in the Soret region is missing in **7a**, apparently having been blue-shifted and possibly becoming the strong absorption at 260 nm. Also, there are weaker maxima at 302, 336, and 438 nm. The following rationalization may account for the strong effect of Sn coordination on the porphyrazine optical spectrum. The Soret transition in porphyrinic molecules is assigned to an $a_{1u} \rightarrow e_g$ ($\pi \rightarrow \pi^*$) transition, where the a_{1u} orbital has its maximum π-electron density on the meso and pyrrole nitrogen atoms. Upon coordination of the tin atom to the meso nitrogen, the energy of this orbital is lowered due to N($p\pi$) → Sn($d\pi$) and/or N → Sn σ-donation. This would widen the energy gap between the ground and excited states and shift the transition to higher energy. Currently, DVM-Xα calculations are being undertaken in order to elucidate the electronic structure of this molecule and to test the validity of this hypothesis.

Interaction of Macrocycles 7a and 7b with Halide and Pseudohalide Anions. When tetraalkylammonium halides or pseudohalides (e.g., F^-, Cl^-, Br^-, I^-, SCN^-) are added to solutions of the di-*n*-butyltin-capped derivative **7b**, the solution undergoes a conspicuous color change from green to purple. Reactions with the halides do not cause destannylation of the macrocycle. This would produce the air-sensitive octathiolate, whereas solutions of the halide-coordinated macrocycle are remarkably air-stable: they remain unchanged for weeks under ambient conditions and deliberate aeration does not cause any spectral changes, precipitation, or other evidence of decomposition. As more poorly coordinating anions (e.g., $CF_3SO_3^-$, NO_3^-, ClO_4^-) do not induce this spectral change, we conclude that it is a result of halide coordination to Sn. Solutions of **7b** in coordinating solvents (e.g., pyridine, di-

(25) (a) Hove, M. J.; Hoffman, B. M.; Ibers, J. A. *J. Chem. Phys.* **1972**, *56*, 3490. (b) Plumlee, K. W.; Hoffman, B. M.; Ibers, J. A.; Soos, Z. G. *J. Phys. Chem.* **1975**, *63*, 1926. (c) Eisenberg, R.; Ibers, J. A. *Inorg. Chem.* **1965**, *4*, 605. (d) Kobayashi, A.; Sasaki, Y. *Bull. Chem. Soc. Jpn.* **1977**, *50*, 2650. (e) Bousseau, M.; Valade, L.; Legros, J.-P.; Cassoux, P.; Garbauskas, M.; Interrante, L. V. *J. Am. Chem. Soc.* **1986**, *108*, 1908, 1916. (f) Underhill, A. E.; Tonge, J. S.; Clemenson, P. I.; Wang, H.-H.; Williams, J. M. *Mol. Cryst. Liq. Cryst.* **1985**, *125*, 439–446. (g) Alvarez, S.; Vincente, R.; Hoffmann, R. *J. Am. Chem. Soc.* **1985**, *107*, 6253–6277 and references therein. (h) Weiher, J. F.; Melby, L. R.; Benson, R. E. *J. Am. Chem. Soc.* **1964**, *86*, 4329. (i) Burgess, J.; Davis, K. M. C.; Kemmitt, R. D. W.; Raynor, J. B.; Stock, J. *Inorg. Chim. Acta* **1970**, *4*, 129.

(26) Gouterman, M. In *The Porphyrins*; Dolphin, D., Ed.; Academic Press: New York, 1978; Vol. 2, Chapter 1.

(27) (a) Lever, A. B. P. *Adv. Inorg. Chem. Radiochem.* **1965**, *7*, 28. (b) Linstead, R. P.; Whalley, M. *J. Chem. Soc.* **1952**, 4839.

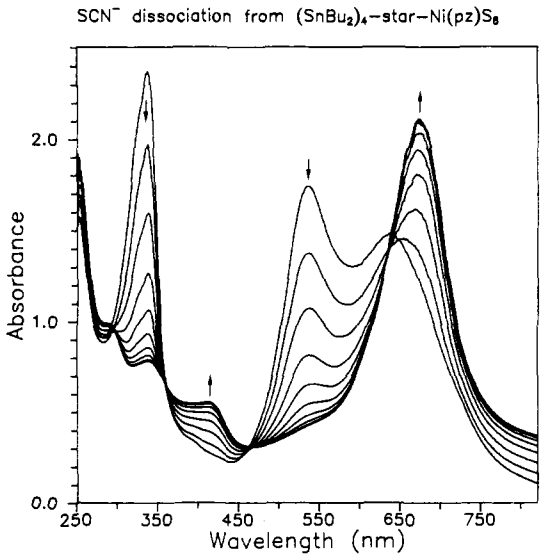

Figure 7. Effect of a 100-fold dilution of a solution of SCN^--coordinated **7b** upon the optical absorption spectra as a function of time. Spectra were recorded in $ClCH_2CH_2Cl$ solvent at 1-min intervals. In this experiment the spectra have ceased changing after 9 min.

methylacetamide, DMSO) also show a similar spectral change, suggesting solvent coordination to tin. The reactivity of the di-*tert*-butyltin capped derivative **7a** is similar to that of **7b** except that **7a** does not show a color change in the presence of I^- or coordinating solvents, presumably because the added steric bulk of the *tert*-butyl groups limits the accessibility of large ligands to the tin coordination sphere.

The changes in the electronic spectrum of **7a** upon progressive additions of F^- are shown in Figure 6. Binding apparently occurs in two stages. The first stage occurs with the addition of up to four F^- ions per macrocycle; it is accompanied by a sharp decrease in the absorbance at 676 nm and a marked increase at 338 nm, with isosbestic points at 300 and 610 nm. During the addition of four more fluoride ions per macrocycle, to a total of 8 equiv, the spectrum changes further: the isosbestic point at 610 nm is lost and three new isosbestic points at 366, 482, and 766 nm are observed; the absorbance at 338 nm continues to increase and two new peaks at 542 and 626 nm appear. The reaction appears to be essentially complete with the addition of eight F^- ions per macrocycle to form an adduct, $\mathbf{9b}(F^-)_8$; addition of a large excess (50 equiv) of fluoride only slightly increases the intensity of the new peaks.

The reaction with fluoride is irreversible; the spectra are measured in dilute solution (2×10^{-5} M) with minimal excess F^-, and further dilution only results in a corresponding decrease in the overall absorption of the spectra. In contrast, the reaction of **7a** or **7b** with more weakly coordinating halides is reversible. Concentrated solutions of **7b** (ca. 10^{-3} M) treated with 20 equiv of Br^-, I^-, or SCN^- are purple, with a spectrum nearly identical to that of $\mathbf{9b}(F^-)_8$, indicating the formation of the corresponding $\mathbf{9b}(X^-)_8$ complex. Diluting these solutions by 1/100 to a concentration suitable for obtaining optical spectra (10^{-5} M) causes the solution color to revert to green with an optical spectrum identical to that of **7b**. Thus, for I^-, Br^-, and SCN^-, but not F^-, the ligand binding is reversible. For I^- the purple to green color change caused by the loss of halide occurs instantaneously upon dilution; for Br^- it occurs over a few seconds. For SCN^- the change is gradual and is complete in 5–10 min. This allows measurement of the time course of the loss of SCN^-, as shown in Figure 7. The spectrum of $\mathbf{9b}(SCN^-)_a$ progresses to that of **7b** with clear isosbestic points at 296, 358, 464, and 632 nm, which are qualitatively similar to those seen in Figure 6.

More detailed studies were conducted using bromide as the coordinating halide. Bromide was chosen because its coordination to the tin atom is reversible (vide supra) and the solutions reach equilibrium quickly. For the simple case of $A + nX \rightarrow AX_n$, the

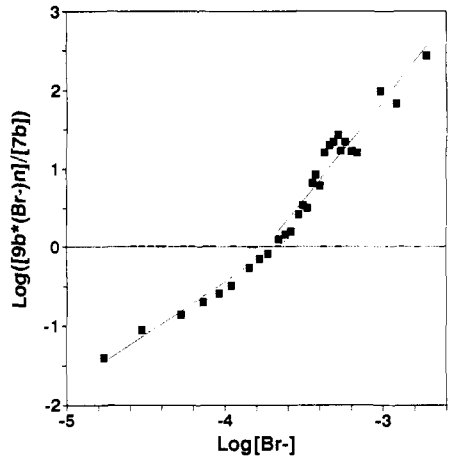

Figure 8. Plot of the logarithm of the reaction coordinate {log ($[\mathbf{9b}\cdot Br_n]/[\mathbf{7b}]_{total}$)} versus log $[Br^-]$ as monitored by the increase in absorbance maximum at 338 nm.

equilibrium can be expressed as $\log([AX_n]/[A]) = n \log [X] + \log K$, thus a plot of $\log([AX_n]/[A])$ versus log [X] would yield a straight line of slope n. A plot of $\log([\mathbf{9b}\cdot Br_n]/[\mathbf{7b}]_{total})$ versus log $[Br^-]$ is shown in Figure 8. The data do not lie on a single straight line, indicating more complex behavior. For lower Br^- concentrations ($[Br^-] < 20[\mathbf{7b}]$) the data can be fit to a straight line with a slope of nearly unity ($n = 1.07$). This is consistent with an initial binding phase in which each tim atom independently binds a single halide ion to form complex $\mathbf{9b}(X^-)_4$, which has a total of four bound halides and six-coordinate tin ions chelated in the tridentate mode. For higher Br^- concentrations ($[Br^-] \geq 20[\mathbf{7b}]$), there is an even sharper rise in the absorption at 338 nm, and the best fit line to this portion of the data has a slope of about $n = 2$, indicating cooperative binding of the Br^- ion. The final spectra for Br^- coordination are identical to those for F^- coordination, so we infer that the second phase involves binding of four additional Br^-, to a final stoichiometlry of $8Br^-$. Much more detailed studies will be required to fully characterize the cooperative two-stage equilibrium binding process and the kinetics of the dissociation process, which apparently exhibits only one stage (one set of isosbestic points) (Figure 7).

We have not yet been able to crystallize either a tetrahalide- or octahalide-coordinated product. However, the number of plausible structures for these complexes is limited. As noted earlier, simple destannylation of the macrocycle can be ruled out because the reaction products are air-stable and the reaction is reversible. A reasonable structure for $\mathbf{9b}(X^-)_4$ would involve the coordination of a single halide ion to each tin atom bound in the tridentate (S–N–S) site (Scheme II). There is ample precedent for six-coordinate tin complexes bearing both thiolate and halide ligands.[28] It is unlikely that the structure of $\mathbf{9b}(X^-)_8$ involves the simple coordination of one more halide ion to each Sn atom of $\mathbf{9b}(X^-)_4$, as this would yield a seven-coordination tin complex, and known higher coordinate tin complexes require the ligation of chelating ligands with small bite angles such as carboxylates. Also, considering the steric demands of the bulky *tert*-butyl groups, the possibility of having seven-coordinate Sn bound at the tridentate site is also unlikely. Instead we suggest that further addition of halide causes the Sn atoms to migrate from the tridentate (S–N–S) site to the bidentate (S–S) site (Scheme II). In the bidentate site, each Sn atom could easily accommodate two halide ligands, forming an octahedral complex without undue steric congestion. One might expect that the spectrum of such a migration product would more closely resemble the spectra of the octakis(alkylthio)porphyrazines because the Sn atoms could no longer interact with meso nitrogen pπ orbitals, and the regener-

(28) Bredtschneider, E. S.; Allen, C. W. *Inorg. Chem.* **1973**, *12*, 623.
(29) Brown, T. G.; Petersen, J. L.; Lozos, G. P.; Anderson, J. R.; Hoffman, B. M. *Inorg. Chem.* **1977**, *16*, 1563.
(30) Harrison, S. E.; Assour, J. M. *J. Chem. Phys.* **1964**, *40*, 365.

Scheme II

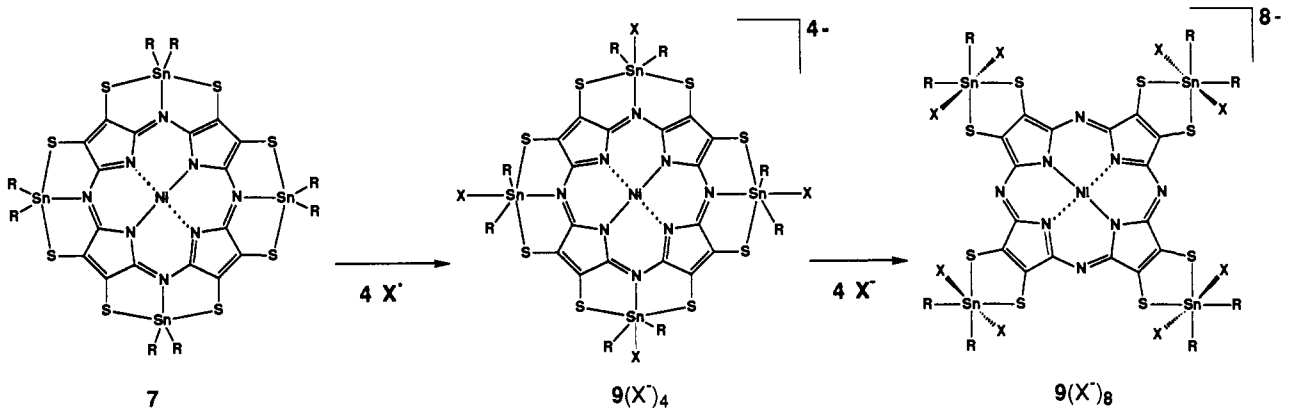

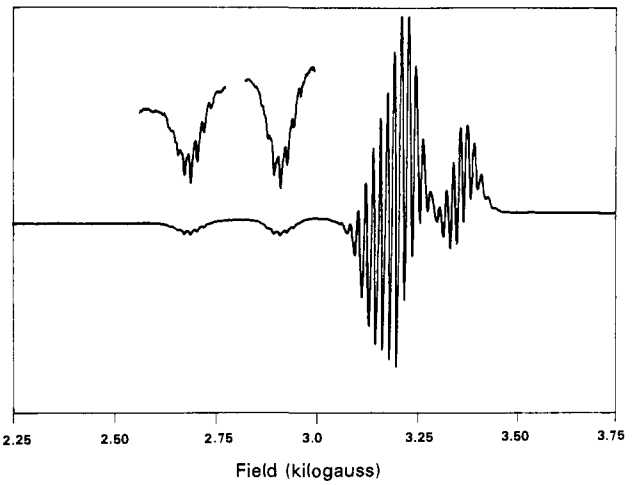

Figure 9. X-band EPR spectrum (9.050 GHz) of 1% Cu-*star*-porphyrazine (**8**) magnetically diluted into Ni host **7a**, recorded at 77 K.

ation of the absorption at 338 nm in the Soret region agrees well with this expectation. Therefore the bidentate structure (Figure 1) is proposed for **9b**. The migration of the four dialkyltin moieties clearly must represent a cooperative process, in agreement with the equilibrium binding curves.

Electron Paramagnetic Resonance. The EPR spectrum at 77 K of a powder sample of 1% Cu-*star*-porphyrazine (**8**) magnetically diluted in its diamagnetic host **7a** is shown in Figure 9. The spectrum shows axial symmetry as is typically seen for monomeric square-planar Cu(II) complexes. The **g**-tensor values are $g_\perp$ = 2.15 and $g_\parallel$ = 2.03, with a hyperfine splitting of $A_\parallel^{Cu}$ = 217 G. In addition, the spectrum shows well-resolved ^{14}N hyperfine coupling due to spin density on the coordinated nitrogen atoms, and this hyperfine structure is also anisotropic. In the $g_\parallel$ region, the hyperfine splitting corresponds to B_N = 15.5 G. The nine-line splitting pattern in the $g_\perp$ region arises from a combination of A_N and B_N, and the observed splitting $B_N' = (A_N + B_N)/2$ which gives A_N = 19.6 G. The *g* values and the Cu and N hyperfine coupling constants of **8** are very near to those of Cu(omtp). This observation suggests that although the coordination of Sn to the macrocycle has a profound effect on the π-electron structure of the porphyrazine rings, its effect on the electronic properties of the Cu^{2+} ion, whose unpaired electron density is in a σ-orbital ($Cu(d_{x^2-y^2}) + N(p\sigma)$), is negligible. Interestingly, the coupling constants and *g* values of **8** and Cu(omtp) are noticeably different from those of Cu(pc) and Cu(tpp) (Table IX).

Table IX. EPR Parameters for Cu-*star*-porphyrazine (**8**) and Related Cu Porphyrinic Macrocycles[a]

complex	$g_\parallel$	$g_\perp$	$A_\parallel^{Cu}$	A^N	B^N
8	2.15	2.03	217	20.5	15.5
Cu(omtp)[9]	2.14	2.06	215	19.9	15.0
Cu(tpp)[29]	2.19	2.03	209	18.9	14.9
Cu(pc)[30]	2.18	2.05	198	18.6	14.2

[a] Hyperfine coupling constants are expressed in units of gauss.

Conclusion

In this work, we have presented the initial findings on the structure and reactivity of the unusual polynucleating porphyrazineoctathiolato ligand. The crystal structure of its di-*tert*-butyltin(IV) complex demonstrates for the first time the ability of the meso nitrogen atoms to coordinate metal ions at the periphery of the macrocycle. This peripheral metal-ion coordination has a profound effect on the electronic structure of the porphyrazine π-system as evidenced by electronic absorption spectroscopy. Halide binding to Sn causes migration of the dialkyltin moieties from the tridentate (S–N–S) binding site to the bidentate (S–S) site has been studied spectroscopically. Work in progress includes structural and spectroscopic characterization of the bidentate binding mode for M^2 = Sn, as well as for transition-metal ions.

Acknowledgment. This work has been supported by the National Science Foundation (Grant DMR-8818599 to B.M.H.) and by the Camille and Henry Dreyfus Foundation (Teacher-Scholar Award to A.G.M.B.).

Registry No. 1, 5466-54-6; **2**, 52626-59-2; **3a**, 129491-57-2; **3b**·H_2O, 141272-54-0; **4**, 129491-60-7; **5a**, 129466-88-2; **5b**, 141272-49-3; **6a**, 129491-58-3; **6b**, 141272-53-9; **7a**, 129491-59-4; **7a**·(C_7H_8)·1.25(CH_2Cl_2), 141318-23-2; **7b**, 141272-52-8; **8**, 141272-50-6; **9a**$(F^-)_4$, 141272-63-1; **9a**$(F^-)_8$, 141272-66-4; **9a**$(Br^-)_4$, 141272-64-2; **9a**$(Br^-)_8$, 141291-98-7; **9a**(SCN^-), 141272-65-3; **9a**$(SCN^-)_8$, 141291-99-8; **9b**$(F^-)_4$, 141272-55-1; **9b**$(F^-)_8$, 141272-59-5; **9b**$(Br^-)_4$, 141272-56-2; **9b**$(Br^-)_8$, 141272-60-8; **9b**$(I^-)_4$, 141272-57-3; **9b**$(I^-)_8$, 141272-61-9; **9b**$(SCN^-)_4$, 141272-58-4; **9b**$(SCN^-)_8$, 141272-62-0; $obtp^{2-}$, 141272-48-2; Mg, 7439-95-4; $(t\text{-Bu})_2SnCl_2$, 19429-30-2; AgNO, 7761-88-8; benzyl bromide, 100-39-0; dibutyltin(IV) dichloride, 683-18-1; dibutyltin(IV) dinitrate, 5072-80-0; di-*tert*-butyltin(IV) dinitrate, 141272-51-7.

Supplementary Material Available: Tables of positional parameters and $U(i,j)$ values for **7a**·(C_7H_8)·1.25(CH_2Cl_2) and positional parameters and anisotropic thermal parameters for **3b**·H_2O (6 pages); listing of structure factors (50 pages). Ordering information is given on any current masthead page.